Physica **40** (1968) 229–252

EXCITATION TO THE METASTABLE STATES AND IONIZATION FROM GROUND AND METASTABLE STATES IN HELIUM

MEASUREMENTS WITH CROSSED ATOMIC AND ELECTRON BEAMS

L. VRIENS, T. F. M. BONSEN and J. A. SMIT

Fysisch Laboratorium der Rijksuniversiteit, Utrecht, Nederland

Received 24 April 1968

Synopsis

We designed a crossed beam apparatus, the new aspect of which is that an atomic beam is subsequently crossed by two parallel electron beams. The first electron beam has the function to produce metastable atoms which are then ionized in the second beam. In this way we measured the energy dependence of the cross sections for ionization of He from the metastable 2^3S and 2^1S states. These measurements require a high ion detection efficiency.

The high sensitivity of the apparatus also enabled us (i) to measure cumulative ionization within one electron beam (and to measure excitation to the 2^3S and 2^1S states of He) and (ii) to very accurately measure the cross section for direct ionization from the ground state. We reduced the effect of thermal energy spread in the electron beam on the latter experimental results using mathematical unfolding techniques. For direct ionization from the ground state of He we obtained the following threshold dependence of the cross section Q_i (in 10^{-16} cm^2) on the electron energy E_e (in eV):

$$Q_i = (8.6 \pm 0.5) \times 10^{-3} (E_e - 24.58)^{1.13 \pm 0.02}$$

for $24.58 \text{ eV} \leq E_e \leq 27.1 \pm 0.3$ eV, and

$$Q_i = 0.0125 [E_e - (25.14 \mp 0.04)]$$

for $27.1 \pm 0.3 \text{ eV} \leq E_e \leq 34$ eV. These formulae agree with experiment within the experimental uncertainty. We cannot decide whether a more complicated formula would give a better fit.

1. *Introduction*

1.1. *General aspects of crossed beam experiments.* In earlier experiments, by various investigators, one electron beam was sent through beams consisting of: (i) neutral hydrogen[1]) or alkali atoms[2]), to study ionization, excitation and elastic collisions, (ii) polarized atoms[2]), to study electron exchange, (iii) excited neutral atoms[3,4]) to measure ionization or "superelastic" collisions, (iv) negative ions[5,6]) to measure electron detachment, and (v) positive ions[7–9]) to measure ionization and excitation. Beams of hydrogen or alkali atoms are usually obtained from ovens[1]) and beams with

excited (metastable) atoms from gas discharges[3, 10]). The new aspect in our work[11]) is that an atomic or molecular beam is subsequently crossed by two parallel electron beams. Metastable atoms are produced in the first electron beam and ionized in the second beam (see section 2).

1.2. *Ionization of metastable helium atoms.* Fite and Brackmann[3]) were the first ones to measure, among other things, ionization of metastable helium. They used a gas discharge to produce a beam with metastable atoms. The chief advantage of a gas discharge is that larger densities of excited atoms can be obtained; the chief advantage of our method[11]) is that the excitation can better be controlled, *i.e.* we can preferentially excite some special states. The two methods are quite different for molecules, because in a gas discharge chiefly low lying vibrational and rotational states are excited, while with our method we preferentially induce electronic transitions. The relative energy dependence we measured for ionization from a mixture of metastable He atoms differs a little from the dependence measured by Fite and Brackmann.

Cross sections for ionization of helium from the metastable states 2^3S and 2^1S have been calculated by Vriens[12]) (see section 3). A fairly good agreement exists between the shape of the theoretical and experimental curves.

1.3. *The threshold behaviour for ionization of He from the ground state.* The threshold behaviour of cross sections for electron impact ionization of atoms and molecules has been the subject of many experimental and theoretical investigations. From an approximate solution of the classical three-body problem, Wannier[13]) came to a threshold "law"

$$Q_i = C(E_e - I)^{1.127} \tag{1}$$

where Q_i is the total ionization cross section, C a constant, E_e the energy of the incident electron, and I the ionization energy; *i.e.*, $E_e - I$ is the excess energy which is divided between scattered and ejected electron. From an approximate solution of the quantum-mechanical three-body problem, Geltman[14]) and later Rudge and Seaton[15]) came to a linear threshold "law"

$$Q_i = C(E_e - I). \tag{2}$$

Unfortunately, no theoretical predictions about the range of validity of the threshold laws were given. In 1954, Hickam *et al.*[16]) measured for ionization of helium a linear $(E_e - I)$ dependence, up to 8 eV above threshold. Hickam *et al.*[16]) write about their ionization function: "It must be noted, however, that this curve covers an energy range of 8 volts and thus may not be a true test of Wannier's law. If the energy range is limited to one or two electron volts, the scatter in the experimental points makes it impossible to determine which of the two power laws gives the best fit to the data". Nevertheless, the linear dependence for helium was accepted in literature and workers in

this field devoted their attention to more complex atoms and molecules. In 1967, however, Brion and Thomas[17]) measured a threshold behaviour which did excellently agree with Wannier's law for about the first two volts above threshold, and with a linear $(E_e - I)$ dependence for the next six volts. Since with our apparatus we can easily measure ionization from the ground state, we thought it worthwile also to study the threshold dependence of Q_1 for helium. The main problem in this sort of work is to get a sufficiently monoenergetic electron beam. Hickam *et al.*[16]) for instance used the RPD (retarding potential difference) method of Fox *et al.*[18]), and Brion and Thomas[17]) worked with an electron spectrometer with 127° electrostatic cylindrical monochromator and analyzer. We analyzed our data with the EDD (energy distribution difference) method of Winters *et al.*[19]) and with the EDD[2] method (see section 8). Our results (see section 4) essentially confirm those of ref. 17.

1.4. *Excitation to the metastable states in He.* Finally, the high sensitivity of our apparatus enabled us to measure cumulative ionization within one electron beam; *i. e.*, to measure excitation to 2^3S and 2^1S near threshold (see section 5). We also applied the EDD method to these results. Many earlier measurements, with different methods, are reported on 2^3S and 2^1S excitation. Maier-Leibnitz[20]) used an electron swarm technique with retarding potentials to select the scattered electrons. Dorrestein[21]) produced the metastables with an electron beam and detected them via secondary electron emission, which occurs when metastables impinge on a metal surface. Later, Schulz and Fox[22]) used the same technique in combination with the RPD method and obtained improved resolution. Very recently, Pichanick and Simpson[23]) further refined Dorrestein's method by using an electron spectrometer with a 180° spherical electron monochromator to produce a monoenergetic electron beam. They measured with energy resolutions (full width at half maximum of energy distribution) of 0.15 eV down to 0.04 eV. Their results are undoubtedly the best ones obtained on total cross sections. Other methods to detect metastables have been employed by Woudenberg and Milatz[24]) (absorption of a suitable spectral line) and Cermak[25]) (Penning ionization and subsequent detection of the ions with a mass spectrometer). With most techniques one measures 2^3S plus 2^1S excitation; exceptions are the absorption technique[24]) and the method used by Holt and Krotkov[26]) (Stern-Gerlach separation of singlets and triplets). Instead of detecting the metastables (refs. 21, 22, 23, 25 and 26) one can also study the inelastically scattered electrons (ref. 20), as is nowadays often done with electron spectrometers, and in this way measure differential cross sections for individual transitions. For helium such differential measurements near threshold are reported by Schulz and Philbrick[27]), Chamberlain and Heideman[28]), and Ehrhardt and Willmann[29]).

2. *Apparatus and its working*

2.1. *General principles.* A schematic drawing of our apparatus is shown in fig. 1. The gas under investigation, for instance helium, is introduced into a gascontainer via a needle valve. The pressure in the gascontainer is variable and is under working conditions 10^{-1} to 10^{-2} torr. The container is connected with the highvacuum part of the apparatus via a long (50 mm) rectangular (1 × 4 mm) channel so that an atomic beam emerges from the channel. Two parallel electron beams are passed through the atomic beam in the source (collision chamber) region of the "high" vacuum part of the apparatus. Metastable atoms are produced in the first beam and ionized in the second beam. The ions are subsequently extracted from the ion source (second collision chamber), accelerated, analyzed in a 60° sector type mass spectrometer and detected with a Daly detector[30]).

2.2. *Atomic beam.* A conventional way to produce an atomic beam is to use a slit system, a "high" pressure on one side, vacuum at the other side and differential pumping between. If the "high" pressure on the entrance side is so low that the mean free path λ_a of the atoms is large

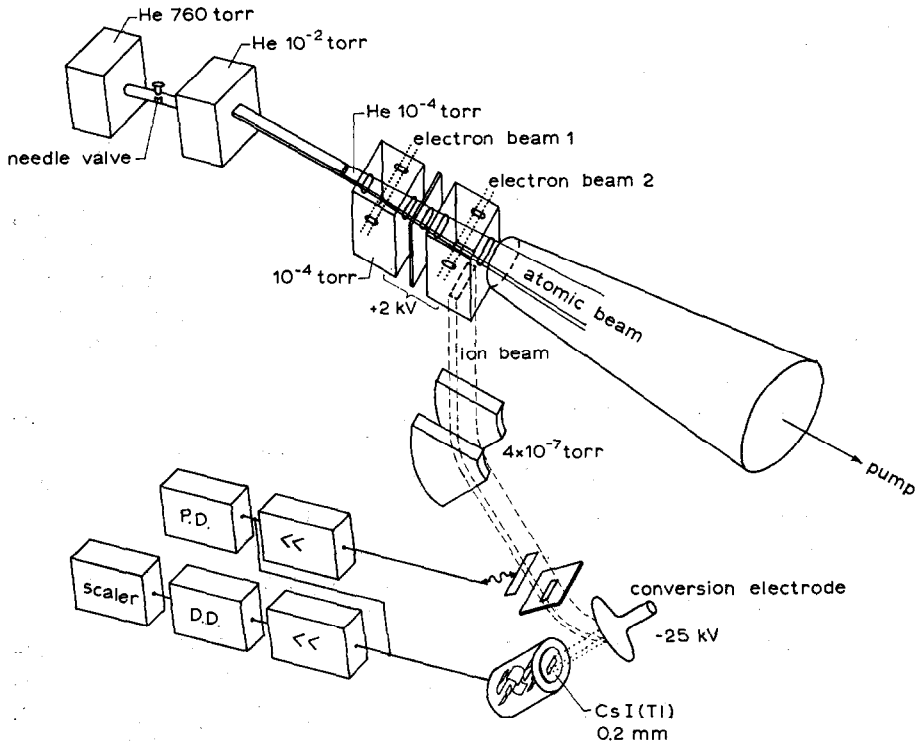

Fig. 1. Schematic drawing of the crossed beam apparatus for the measurement of ionization of metastable atoms.

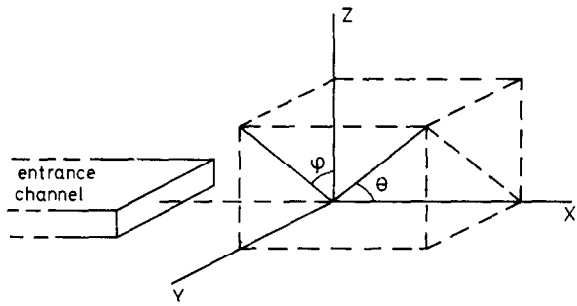

Fig. 2*a*. Angular intensity distribution in the atomic beam; choice of coordinate system. The atomic beam emerges from the entrance channel and is directed along the positive X axis.

compared to the width of the first slit, then the intensity distribution on the low pressure side of this slit is a cosine distribution. The next slits cut the central part out of this broad distribution. Because $\cos\theta$ varies slowly for small θ, the density distribution in the atomic beam is very homogeneous. However, only small densities of atoms can be obtained with this method.

With a rectangular channel, the density distribution is not so very homogeneous, but larger beam intensities can be obtained and no differential pumping system is used. If λ_a is large compared to the width (height) of the channel, there is molecular (Knudsen) flow through the channel and we can rather accurately calculate the total (neutral) beam current and intensity distribution. Von Smoluchowski[31]) calculated the total flow for this case. The intensity distribution has been calculated before only for a cylindrical channel[32]). In his calculation, Clausing[32]) made three assumptions: (i) there is molecular flow, (ii) the reflection of atoms from the tube walls follows a cosine law, and (iii) there are no temperature gradients. We used Clausing's technique* to calculate the intensity distribution for our channel ($1 \times 4 \times \times 50$ mm). The results are shown in fig. 2. The distributions of fig. 2 (*b* and *c*) correspond to the directions in which the atoms come from the exit opening of the channel. Because the width of the channel (1 mm) is not small compared to the width of the electron beam in the second collision chamber (see section 2.3), the actual density distribution of the atoms in the second electron beam will be broader and thus more homogeneous than expected from fig. 2.

For a (helium) pressure of 10^{-2} torr and $T \approx 300°$ K at the entrance side of the channel, $\lambda_a = 14.7$ mm and the average density of the atoms at the exit side of the channel corresponds to a "pressure" (at 300°K) of 10^{-4} torr (calculated using the well known formula for the conductance of a rectangular channel for molecular flow). For 10^{-1} torr at the entrance side, the

* We are indebted to H. Wallinga, for working out many details of this problem.

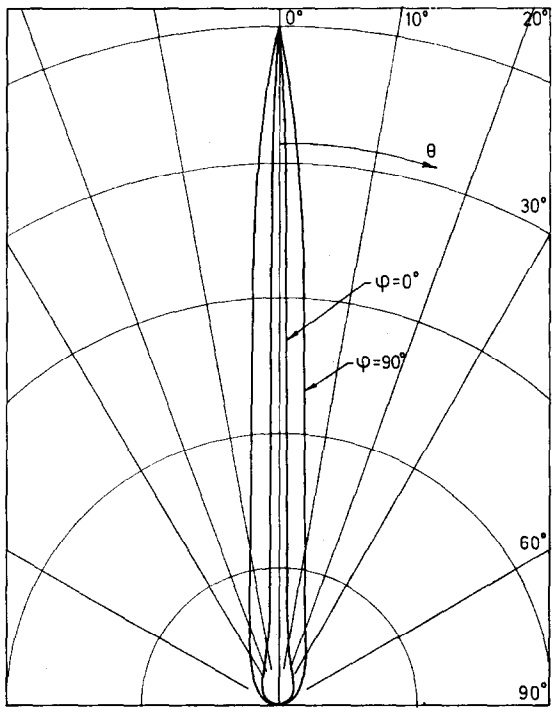

Fig. 2*b*. Angular distribution in the atomic beam; intensity per unit solid angle in direction (θ, φ) for $\varphi = 0°$ and $\varphi = 90°$.

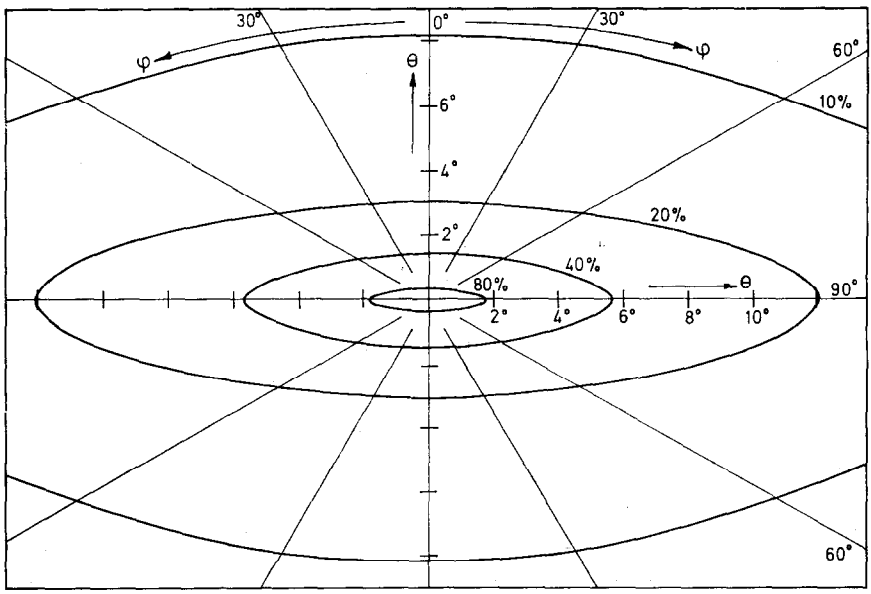

Fig. 2*c*. Angular distribution in the atomic beam; plot with lines of constant intensity for $I(\theta, \varphi) = 80\%$, 40%, 20% and 10% of the forward intensity $I(0, \varphi)$.

condition for molecular flow is less well satisfied and the beam emerging from the exit side will be slightly broader than the calculated one.

2.3. *Collision region.* A schematic drawing of the collision region is shown in fig. 3*. The whole collision region, *i.e.* shield 1 (S_1) and everything within S_1, is kept at about +2 kV with respect to the rest of the mass spectrometer (this 2 kV is needed to focus and accelerate the ion beam). Electrons emitted by tungsten filaments are accelerated through a slit (of 5 × 1 mm in the metastable source and 4 × 0.5 mm in the ion source) to the collision chamber (c_1 or c_2). The dimensions of entrance and exit slits of the collision chambers are 2.4 × 5 mm (c_1) and 1.5 × 5 mm (c_2). The dimensions of the corresponding entrance "slits" of the anodes are 3 × 6 mm (a_1) and 2 × 6 mm (a_2). A magnetic field of about 100 gauss is used to collimate the electron beams; with this magnetic field the electron currents on the walls of the collision chambers c_1 and c_2 are negligible compared to those measured on the anodes a_1 and a_2. The magnetic field simultaneously prevents electrons from wandering from one to another collision chamber. We keep S_2 about 1 V positive with respect to c_1; because of this potential difference, ions formed in c_1 cannot penetrate into c_2. We further give a_1 and a_2 potentials which are about 0.2 V higher** than those of c_1 and c_2 respectively. The ions are extracted from c_2 by a small extraction field (j_0 is usually kept at about −1 V with respect to c_2) and focussed by adjustable potentials on j_1, j_2, j_3 and D (j_1, j_2 and j_3 are usually kept at about −10 V with respect to c_2).

2.4. *Operating pressures.* The collision chamber region is separated from the mass spectrometer by a wedge-shaped channel which acts as a pumping resistance. Only about 3% of the total gas-flow through the entrance channel is pumped away via the mass spectrometer; the other 97% is pumped away via a conical channel placed opposite the entrance channel. When no gas is introduced, the pressure everywhere in the system is lower than 2×10^{-7} torr. With $p \approx 10^{-1}$ torr helium in the gascontainer we measured $p \approx 5 \times \times 10^{-7}$ torr in the mass spectrometer. For this situation the (calculated) density of the effective part of the atomic beam in the collision chambers corresponds to a pressure of about 6×10^{-6} torr and the measured background pressure in the source region is about 10^{-4} torr. The distances

* The dimensions of the collision chamber system were chiefly determined by the dimension of the mass spectrometer (which was originally used for another purpose) to which our system was connected.

** To give a_1 and a_2 slightly higher potentials than c_1 and c_2 has the advantage that slow secondary electrons cannot come back in c_1 and c_2. Especially because these slow electrons can be trapped in the collimating magnetic field they might otherwise give rise to disturbing space charge effects. On the other hand the potential differences between anodes and collision chambers should be sufficiently small to avoid field penetration.

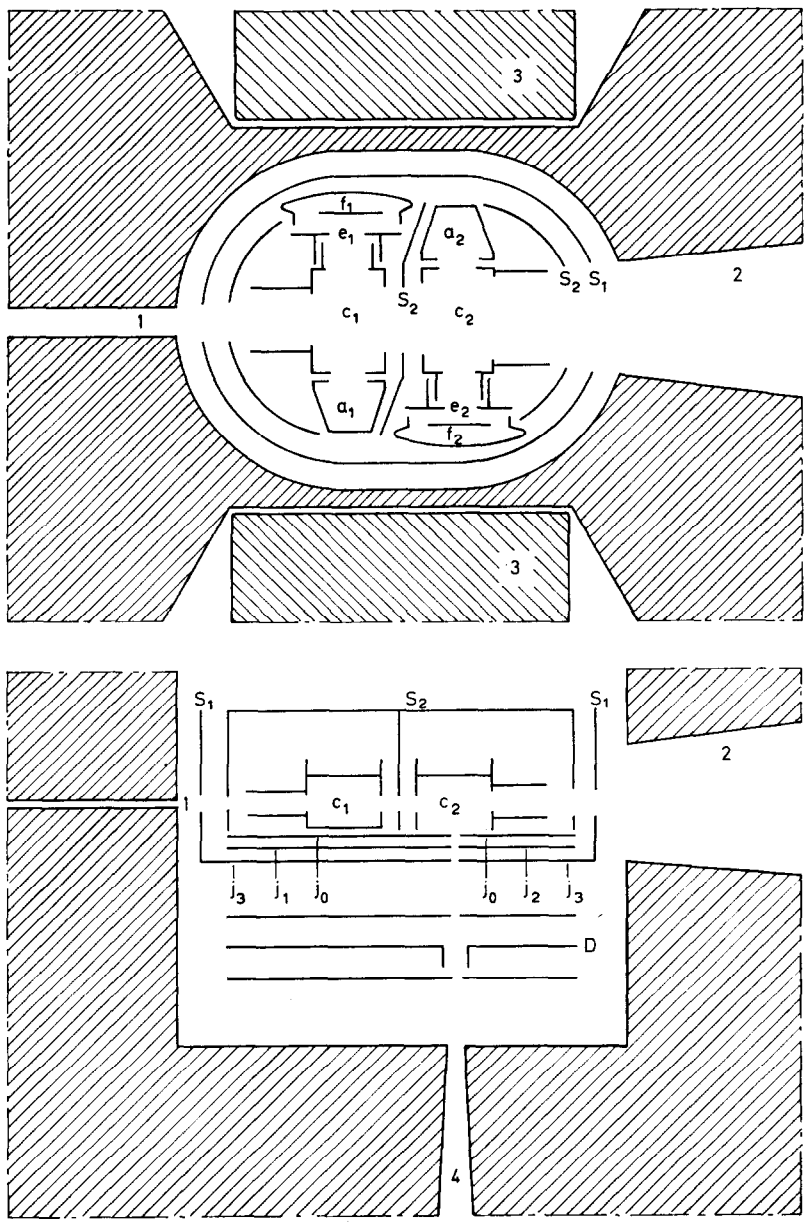

Fig. 3. Upper view and side view of the collision chamber region; 1. entrance channel for atomic beam; 2. conical exit channel; 3. collimating magnet; 4. wedge-shaped pumping resistance in the mass spectrometer; S_1 and S_2 shield electrodes; f_1 and f_2 filaments; e_1 and e_2 accelerating electrodes; c_1 and c_2 collision chambers; a_1 and a_2 anodes; j_0, j_1, j_2, j_3 and D mass spectrometer entrance electrodes to extract, accelerate and focus the ion beam (S_1 has the same potential as j_3). The metal wall surrounding the vacuum system is only schematically indicated; in reality it has a complicated structure and is much thinner than suggested by the figure.

between the exit of the atomic beam channel and the first electron beam and between the electron beams are 24 and 16 mm respectively; because the atomic mean free path $\lambda_a \approx 1500$ mm for $p(\mathrm{He}) = 10^{-4}$ torr, we may neglect collisions of beam atoms with background gas as well as mutual collisions between beam atoms. In measuring cumulative ionization with two electron beams, the atomic beam is still more than 5 times as effective as the background gas, because "beam metastables" preferentially (see section 2.6) go through the "ionizing" electron beam while "background metastables" emerge in nearly arbitrary directions from the first electron beam.

2.5. *Mass spectrometer.* Mass selective detection must be employed in measuring ionization of metastable atoms, because the concentration of impurities (e.g. N_2 and O_2) cannot be kept small with respect to the concentration of metastables. For helium, for example, we estimate that under usual working conditions (see section 3) a fraction of 10^{-7} to 10^{-6} of the ground state atoms in the effective part (where the electrons pass through) of the atomic beam is excited to metastable states. The density of metastable atoms in the ionizing electron beam then corresponds to a pressure (at 300°K) of, for example, 2×10^{-13} torr. Many impurities will be present in higher densities and they have ionization energies between 12 and 16 eV. Consequently, for electron energies above 12 eV, ionization of impurity atoms (molecules) can easily give much larger ion currents than ionization of metastable helium.

Because of the low concentration of metastable He, the corresponding ion current is very small ($< 10^{-18}$ A at the detector) and the mass spectrometer must be very sensitive. We use a conventional 60° sector type mass spectrometer with a Daly detector[30]). In our Daly detector the ions are accelerated from 2 keV to about 28 keV to a conversion electrode. The produced secondary electrons are accelerated to a 0.2 mm thick CsI(Tl) scintillator mounted on an EMI photomultiplier type 9524S (selected for low dark current). By using counting techniques and pulse-height discrimination, we distinguish between the "low" energy background pulses from the detector and the "high" energy pulses caused by the ions (via the secondary electrons). Under working conditions we measure about 70% of the "ion pulses" with a noise level of 1 to 3 counts per second (dependent on the sort of measurements).

2.6. *Recoil.* Before presenting our experimental results, we discuss an important problem in measuring with two electron beams: the recoil momentum that the atoms receive when they are excited by an electron. We denote mass, initial momentum and initial (kinetic) energy of the atom by M, $\boldsymbol{p}_a$ and E_a and the same quantities of the electron by m, $\boldsymbol{p}_e$ and E_e. If (see fig. 4) the atomic beam is directed along the positive x axis and the

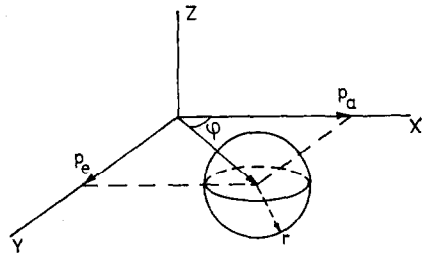

Fig. 4. Illustration of the recoil problem. The atoms initially have momentum $p_a = (2ME_a)^{\frac{1}{2}}$ and the electrons initially have momentum $p_e = (2mE_e)^{\frac{1}{2}}$. The possible momentum vectors $\boldsymbol{p}'_a$ of the excited atoms go from the origin to the surface of the sphere with radius $r = [2m(E_e - E + E_a - E'_a)]^{\frac{1}{2}}$, where E is the excitation energy. For $r = 0$, $\boldsymbol{p}'_a = \boldsymbol{p}_a + \boldsymbol{p}_e$.

electron beam along the positive y axis, then straightforward application of the laws of conservation of energy and momentum shows that

$$(p'_{ax} - p_a)^2 + (p'_{ay} - p_e)^2 + p'^2_{az} = 2m(E_e - E + E_a - E^1_a) \qquad (3)$$

where E is the excitation energy and p'_{ax}, p'_{ay} and p'_{az} are the components of the final momentum of the atom. Here, $E_a - E'_a$ will be very small. Hence, $r^2 = 2m(E_e - E + E_a - E'_a)$ is almost zero for electron energies just above threshold and increases with increasing E_e. For electron energies just above threshold r is small compared to p_e and the (average) change in direction of the atoms in the plane formed by the atomic beam and the electron beam is given by (see fig. 4)

$$\tan \varphi = p_e/p_a = (mE_e/ME_a)^{\frac{1}{2}}. \qquad (4)$$

For larger E_e, *i.e.* when r becomes comparable to p_e, this need not to be true anymore. The probability distribution of different recoil-momenta and thus the probability distribution on the surface of the sphere with radius r are not known. For thermal helium atoms with $E_a \approx 0.04$ eV and $M/m \approx \approx 7400$, the angle φ of eq. (4) changes from about 15° for $E_e = 21$ eV to about 18° for $E_e = 30$ eV. Hence, φ is nearly independent of E_e. However, the radius r strongly varies with E_e and correspondingly, the angular distribution of metastables is very much dependent on the energy of the exciting electrons. We were, probably for this reason, unable to measure the excitation function of the metastable states in helium with two electron beams. Because $\tan \varphi \sim M^{-\frac{1}{2}}$, the recoil problem becomes less severe for heavier atoms or molecules.

3. *Ionization of helium from the metastable states*

To measure absolute cross sections directly, it would be necessary to know the absolute density distribution of the metastables in the atomic beam, the absolute density distribution of the electrons in the (second)

electron beam (for each energy) and the absolute efficiency of the mass spectrometer. The present experimental setup permits only measurement of relative cross sections.

Relative measurements can be made using constant operating conditions, *i.e.* a constant metastable density in the second collision chamber and a constant efficiency of the mass spectrometer (with constant we mean independent of the electron energy in c_2). Since the electron energy in c_2 is a variable, one wants to establish such conditions that the electron beam profile in c_2 does not appreciably change with different energies (for details see section 3.1).

3.1. *Experimental conditions.* We measured ionization from the metastable states under various circumstances. In each series of measurements we worked with constant gas supply, constant potentials on (see fig. 3) S_1, S_2, f_1, e_1, c_1, a_1, c_2, a_2, j_0, j_1, j_2, j_3 and D and with a constant collimating magnetic field. Hence the first electron beam and therefore also the metastable production and the density distribution of the metastables in c_2 are constant.

The energy of the electrons in c_2 is varied by changing the potentials on f_2 and e_2, with $V_{e2}-V_{f2}$ kept constant at 3 V. Within the experimental accuracy (about 2%) we then find no variation in I_{a2} (electron current on a_2) when varying $V_{c2}-V_{f2}$ from 3 to 20 V. As mentioned before, I_{c2} was always negligible compared to I_{a2}. For these reasons and because we always worked with low electron currents ($I_{a2} \leq 10$ μA), to reduce space charge effects*, we estimate that the density-distribution in the second electron beam is predominantly determined by the dimension of the slit in e_2, by the collimating magnetic field and by $V_{e2}-V_{f2}$ (= 3 V), and not by $V_{c2}-V_{f2}$. Furthermore, the atomic beam is broader than the electron beams (see section 2.2) and the first electron beam is broader than the second electron beam (see section 2.3). In addition, the produced metastables receive a recoil-momentum which makes the intensity distribution of the metastables in c_2 more homogeneous than the corresponding distribution for ground state atoms. For the above reasons, the ion production from metastables in c_2 will not largely depend on the width (0.5 to 1 mm) of the second electron beam. Because an extraction field of 1 V is used, the efficiency of the mass spectrometer will not largely change with small variations of the width of the second electron beam (resulting in small changes of the places

* We estimate that for $E_e = 4$ eV and $I_{a2} = 10$ μA, space charge may give energy shifts and differences of about 0.2 eV. Due to negative space charge, the electron energy E_e is lower than $V_{c2}-V_{f2}$. The measured ionization threshold is then shifted to a slightly higher energy. Space charge effects become less significant at higher E_e (with constant I_{a2}); *i.e.* their influence reduces with $E_e^{-\frac{1}{2}}$ because the electron density is inversely proportional to the electron velocity.

where the ions are formed in c_2). Consequently, small changes in the density-distribution of the electrons in the second electron beam with varying E_e need not to affect the accuracy of the measured (relative) ionization efficiency curves.

A second source of possible errors is the recoil-momentum that the metastables receive when they are ionized by an electron of the second beam. Equation (3) is again applicable, but now the energy transfer E is not a fixed excitation energy; E can have any energy between the threshold energy I (for ionization from one of the metastable states) and the initial electron energy E_e. In general, however, small energy transfers are more probable than larger ones. Fig. 4 also remains applicable but now r^2 is variable: approximately between zero and $2m(E_e - I)$. A very fortunate circumstance in our experiment is that the two electron beams are anti-parallel. Therefore the main components of the recoil momenta, *i.e.* $\boldsymbol{p}_{e1}$ and $\boldsymbol{p}_{e2}$ have opposite

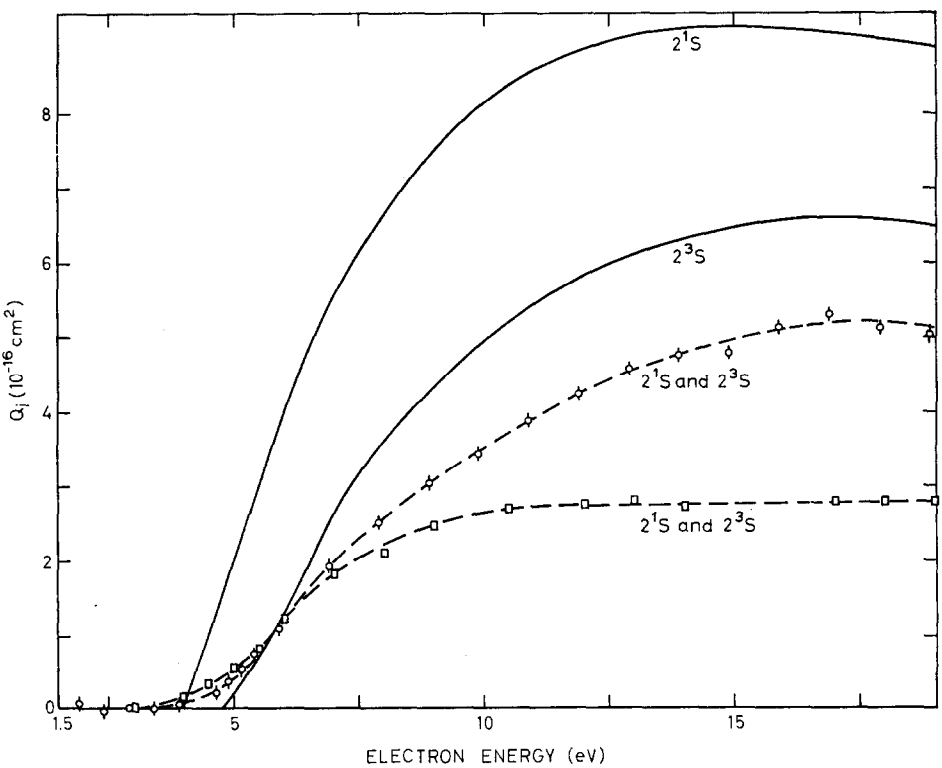

Fig. 5. Experimental cross sections for ionization of an unknown mixture of He 2^3S and 2^1S, and "theoretical" cross sections for 2^3S and 2^1S ionization. Squares: experiment Fite and Brackmann[3]); open circles: present experiment; solid curves: theory, see Vriens[12]). Our (relative) experimental curve has been put in a somewhat arbitrary (see text) way between the other (absolute) cross sections.

directions and partially cancel each other. The remaining component r is small compared to p_a and has a more or less arbitrary direction. Because of the extraction field, which was varied between 0.8 and 1.2 V, we can probably neglect the possible small energy-dependent errors caused by differences in the recoil at smaller or larger E_e.

3.2. *Results.* In fig. 5 we show our experimental efficiency curve for ionization from the 2^3S and 2^1S states. This curve is an average over four series of measurements, which were taken under different circumstances. In the different series of measurements we worked with different I_{a1} (from 15 to 30 μA) and with different pressures. Within the statistical errors our relative efficiency curves were independent of I_{a1} and of the pressure, as should be the case. In all series of measurements I_{a2} was about 10 μA (the statistical errors became too large at smaller I_{a2}). Further, $V_{e1}-V_{f1}$ was 10 V, V_{c1} and V_{c2} were kept at the same potential and V_{S2} was kept at about +1 V with respect to V_{c1}. Separate check measurements showed that the measured ion currents were independent of small (*e.g.* 1 to 2 V) changes of $V_{c2}-V_{c1}$ and $V_{S2}-V_{c1}$ provided that $V_{S2}-V_{c1} > 0.5$ V. With smaller or negative $V_{S2}-V_{c1}$, positive ions formed in c_1 could penetrate in c_2 which resulted in larger ion currents at the detector.

In all measurements we had to subtract "background currents" from the signal. Background currents are caused by different effects. First, when both filaments in the collision chambers are not heated and thus no charged species and no ion beam can be formed in the collision chamber region, we always measured a background current of about 2×10^{-20} A. This current is essentially due to the detector. Second, when both filaments are heated to the usual working temperature but the accelerating potentials ($V_{c1}-V_{f1}$ and $V_{c2}-V_{f2}$) are so low that no cumulative nor direct ionization can occur in c_1 and c_2, we measured an additional background at the detector of about 10^{-19} A. This latter background must be ascribed to ions coming from somewhere in the collision region, but we don't precisely know how they are formed. In our measurement of the ionization function, we determined the total background by lowering $V_{c1}-V_{f1}$ (with $V_{e1}-V_{f1}$ kept constant) to about 17 V (the threshold energies for 2^3S and 2^1S excitation are 19.82 and 20.61 eV, respectively). Fortunately the total background is almost independent of $V_{c1}-V_{f1}$ between 5 and 18 V, so that we are confident it does not change appreciably between 18 and 23 V; usually we work with accelerating potentials in c_1 from 20 to 23 V. Further, the background current was almost independent of I_{a1} between 15 and 30 μA, so that our signal to background (noise) ratio was better at larger I_{a1}. Typical values for signal (ion current + background) to background ratios were 2 and 4, for E_e in c_2 larger than 9 eV. The energy scale of fig. 5 was calibrated against the threshold for ionization from the ground state (see section 4).

In the atomic beam we varied the concentration of triplet metastables with respect to the concentration of singlet metastables by varying $V_{c1}-V_{f1}$ in different series of measurements from 20.5 to 23 V. Namely, the 2^3S excitation function rises rapidly from threshold (19.82 eV) to a maximum at about 20.3 eV (see section 5) and then rapidly decreases again. The 2^1S excitation function has its onset at 20.61 eV and reaches a maximum near 21.0 eV but then for the next few volts the 2^1S cross sections do not change appreciably. Hence at 20.5 eV we preferentially excite triplet metastables and at 23 eV singlet metastables. We could, however, not observe differences in the measured ionization efficiency curves for different $V_{c1}-V_{f1}$. We apparently have the situation that if we work with low I_{a1} our statistical errors are too large, and if we work with larger I_{a1} the energy spread in the first electron beam is too broad.

In fig. 5 we compare our curve with "theoretically (empirically)" calculated[12]) absolute cross sections for ionization of 2^3S and 2^1S atoms and we compare with the absolute cross sections measured by Fite and Brackmann[3]). Fite and Brackmann's curve corresponds (just as our curve) to ionization from an unknown mixture of metastable helium atoms. The experimental curves have a tail near threshold due to energy spread in the second electron beam. Part of the tail may be due to the fact that we measure a (in some way) weighted average of two ionization functions (2^3S and 2^1S) with different thresholds. Also, these ionization functions need not to be linear near threshold. The energy independence of Fite and Brackmann's curve[3]) between 11 and 24 eV (constant Q_i) seems a little unrealistic. Concerning the theoretical curves, these were calculated[12]) using a "classical" formula of Gryzinski. This formula is rather empirical but often gives quite good results. For example, for electron energies between threshold and about 20 times the threshold energy it gives cross sections which are correct within about 10 to 20% for ionization of H, H_2, He, Ar, Kr and Xe. For the alkali atoms the formula gives cross sections which are probably a factor 1.5 to 2 too high and for mercury this factor is about 1.5. For Ne the agreement is poor, at an electron energy twice the threshold energy, the classical formula gives cross sections which are a factor 5 too high. The reason for this exceptional behaviour for Ne is known. For He 2^3S and 2^1S we believe that the correct cross sections lie between the "theoretical" ones of fig. 5 and those which are a factor 2 lower. Our relative experimental curve has been put somewhat arbitrarily in the middle of this region. Since 1964, many other and better justified classical and binary-encounter formulae are given, see for example ref. 33. These much less empirical formulae do, however, not give much better results, for which reason we did not calculate new theoretical cross sections in this way.

4. *The threshold for ionization of helium from the ground state*

When filament f_1 is not heated and consequently there is no electron beam in c_1, we can use our apparatus as a conventional mass spectrometer. In this way we measured the threshold behaviour for ionization of helium from the ground state. Since we did not find any difference in the measured ionization efficiency when varying the extraction field (between 0.8 and 1.2 V) errors caused by the recoil probably can be neglected. Since we took our data with electron currents (I_{a2}) from 2 to 4 μA and electron energies larger than 21 V, space charge effects can completely be neglected. The energy spread in the electron beam is therefore thermal; *i.e.* corresponds to the temperature T of the emitting surface of the filament. Further, since we use a collimating magnetic field, we do not select between electrons which escape in different directions from the emitting surface. In this case the (total*) energy distribution of the emitted electrons is semi-Maxwellian:

$$f(E'_e)\,dE'_e = \beta^2 E'_e \exp(-\beta E'_e)\,dE'_e, \tag{5}$$

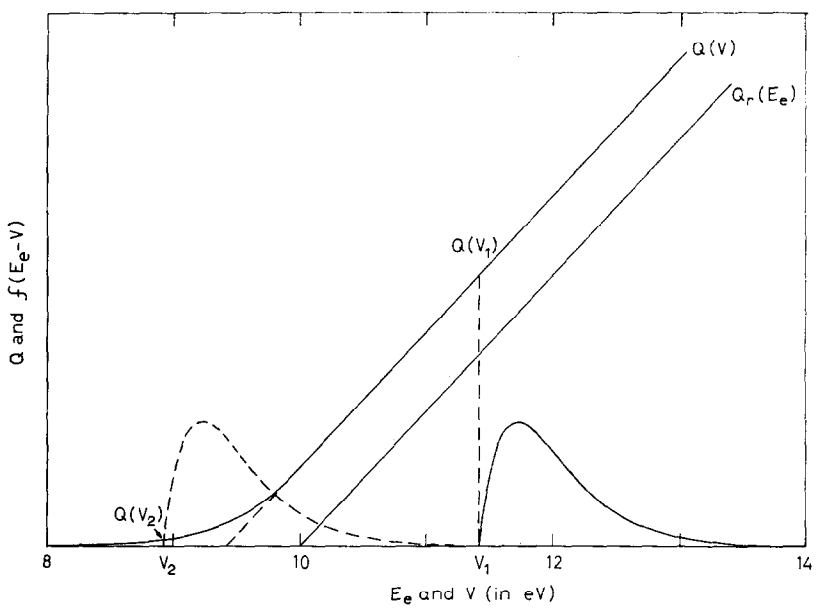

Fig. 6. Illustration of the influence of thermal energy spread in the electron beam on the experimental ionization function. $Q_r(E_e)$ is an (assumed) real ionization function, where E_e is the electron energy and where the threshold energy I is assumed to be 10 eV. $Q(V)$, the measured cross section at accelerating energy V, is obtained by integrating the product of $Q_r(E_e)$ and the electron energy distribution (in the figure a thermal distribution with $kT = 0.3$ eV).

* With total we mean: integrated over all emission angles.

where $\beta = (kT)^{-1}$ and $E'_e \geq 0$. After being emitted, the electrons are accelerated to c_2 and all receive an additional kinetic energy $V = e(V_{c2} - V_{f1})$. Hence the new energy distribution of the electrons in c_2 is

$$f(E_e - V)\, dE_e = \beta^2 (E_e - V) \exp[-\beta(E_e - V)]\, dE_e, \tag{6}$$

where $E_e (\geq V)$ is the electron energy in c_2. Due to this energy distribution, the measured ionization function differs from the real one in two aspects: (i) it is shifted to lower energy and (ii) it has an unrealistic exponential "tail" at the threshold. This is illustrated in fig. 6. From the measured exponential tail one can directly determine kT (between 0.23 and 0.3 eV in our measurements) so that the distribution (6) is precisely known. In this case one can apply unfolding techniques to the experimental results and in this way reduce the effect of the thermal energy spread. In analyzing our measured ionization function, we used two different unfolding techniques: the EDD method[19]) (energy distribution difference method) and the EDD² method. The two methods are described in detail in section 8. In fig. 7 we show the EDD and EDD² electron energy distributions, *i.e.* those distributions which would give the same result as the EDD and EDD² methods. In fig. 7 we also plotted the real distribution, according to eq. (6).

Fig. 8 shows one of our measured efficiency curves, for ionization of He

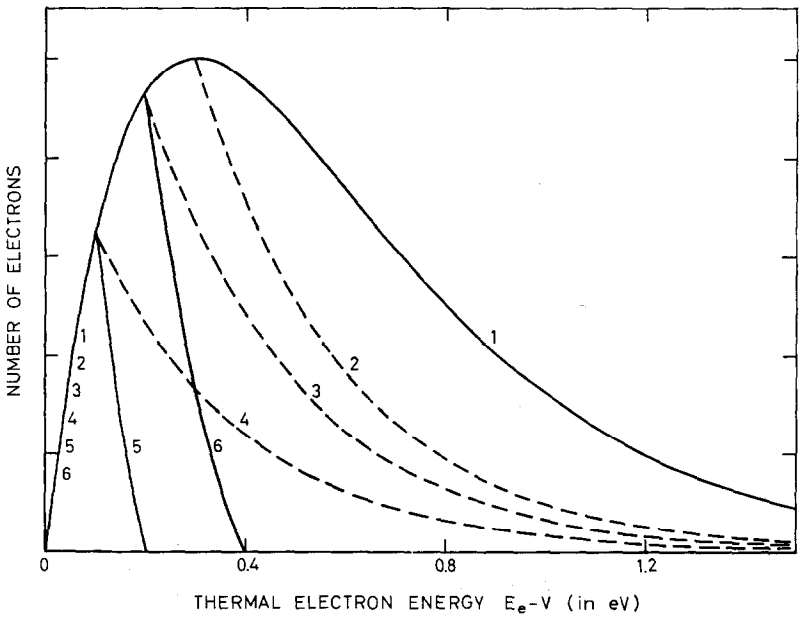

Fig. 7. Electron energy distributions; 1. thermal distribution with $kT = 0.3$ eV; 2, 3 and 4. EDD energy distributions (see text) with $\Delta V = 0.3$, 0.2 and 0.1 eV, respectively; 5 and 6. EDD² energy distributions with $\Delta V = 0.1$ and 0.2 eV, respectively.

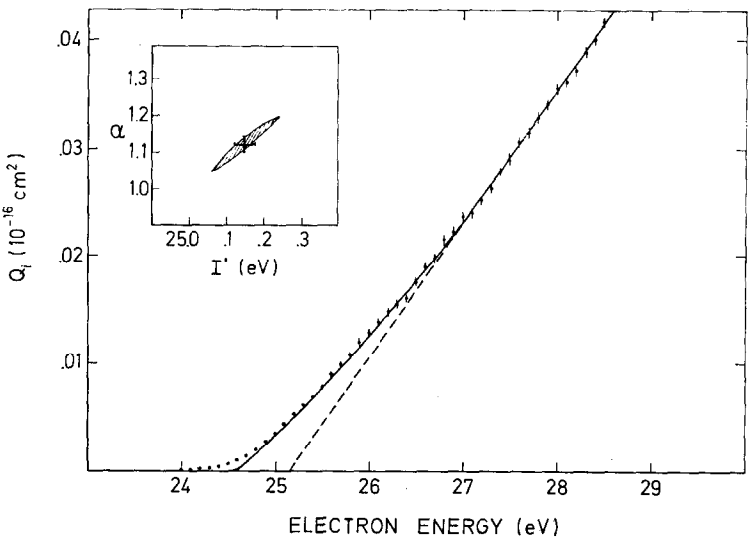

Fig. 8. Cross sections for ionization of He from the ground state. The points in the figure give our experimental results and the solid curve is obtained after unfolding with the EDD[2] method. The unfolded ionization function has been shifted along the energy axis, so that its threshold now has the correct value 24.58 eV. Next, the set of experimental points has been shifted so that they coincide with the unfolded curve in its linear part. The linear part extends up to about 34 eV. The cross sections have been put on an absolute basis using (see text) the absolute cross sections of Rapp and Englander-Golden[35]). The shaded area in the inset of the figure indicates the region of (according to our experimental results) possible α-values (see eq. (7)) and the corresponding possible values of the intersection I' of the linear part of the ionization function with the energy axis.

from the ground state, along with the results obtained with the EDD[2] method. Fig. 8 and all our other experimental results show (after unfolding with EDD and/or EDD[2] methods) that the ionization function for He is essentially nonlinear for about the first 2.5 eV above threshold (24.58 eV). Between 2.5 and about 10 eV above threshold we found no departure from linearity. The nonlinear part of the ionization function near threshold could very well be fitted to Wannier's law (eq. 1). To reach this conclusion, we fitted the coefficients I^*, α and C of the formula

$$Q_i = C(E_e - I^*)^\alpha \tag{7}$$

in the best possible way to the unfolded ionization function. Due to contact potentials, and shifts caused by the energy distribution in the electron beam, I^* will in general not coincide with the ionization energy I. In the fitting procedure we assumed that the nonlinear and linear parts of the ionization function join smoothly. Our results are:

(i) $\alpha = 1.13 \pm 0.02$ (Wannier's value is 1.127).

(ii) The linear part of the ionization function, when extended to lower E_e, intersects the energy axis at 0.56 $\pm$ 0.04 eV above the ionization threshold, thus at 25.14 $\pm$ 0.04 eV.

Before plotting our results in fig. 8, we shifted our measured and unfolded ionization functions along the energy axis in such a way that the linear parts intersect this axis at 25.14 eV. Finally, we normalized our relative cross sections using the absolute (experimental) cross sections of Rapp and Englander-Golden[34]; *i.e.* from the linear part of their ionization function we obtained a slope $dQ_1/dV = 0.0125 \times 10^{-16}$ cm^2/eV and we gave the linear part of our curves the same slope.

5. *Excitation to the metastable states*

In the same mode of operation of the apparatus as described in section 4, thus without electron beam 1, we measured cumulative ionization (within electron beam 2) between 19 and 21 eV: $He(1^1S) \rightarrow He(2^1S \text{ or } 2^3S) \rightarrow He^+$. The ion current resulting from this process is superimposed on the exponential tail for direct ionization, but this exponential tail decreases sufficiently rapidly towards lower E_e and is negligible below 21 eV. The cumulative ion current measured with $I_{a2} = 4\mu A$ and $V_{e2} - V_{f2} = 5$ V is shown in fig. 9. Within the statistical errors this ion current was proportional to $(I_{a2})^2$ for $2\mu A \leq I_{a2} \leq 10\ \mu A$, but above 6 μA the structure in the curve was gradually smeared out, probably by energy spread due to space charge in the magnetically confined electron beam. On the contrary, the ion current for $E_e > 22$ eV was proportional to I_{a2} as should be the case for direct ionization from the ground state. We also applied the EDD method to this case. The resulting curves, corresponding to different energy spreads (see section 8), are also shown in fig. 9. All curves are plotted on an arbitrary vertical scale. However, for each separate curve we adjusted the energy scale against the now known (section 4) intersection of the linear part of the (direct) ionization function with the energy axis.

The cross sections for excitation to the metastable states rapidly vary with E_e for $19.8 \leq E_e \leq 21$ eV. These E_e values are 4 to 5 times as large as the threshold energy for ionization from the metastable states. In this region we do not expect any strong variation of the ionization cross sections (see fig. 5). Our curves in fig. 9 correspond therefore with the excitation function of the metastable states. In fig. 10 we compare (also on an arbitrary vertical scale) two of our unfolded curves with the best experimental ones available on total cross sections, *i.e.* those of Pichanick and Simpson[23] and of Schulz and Fox[22]. The places of first maximum and first minimum of curve 2 agree well with those of refs. 22 and 23. The position of curve 1 on the energy scale is not so good, probably because this series of measurements was interrupted.

It is interesting to note that if we take 24.58 instead of 25.14 eV as the

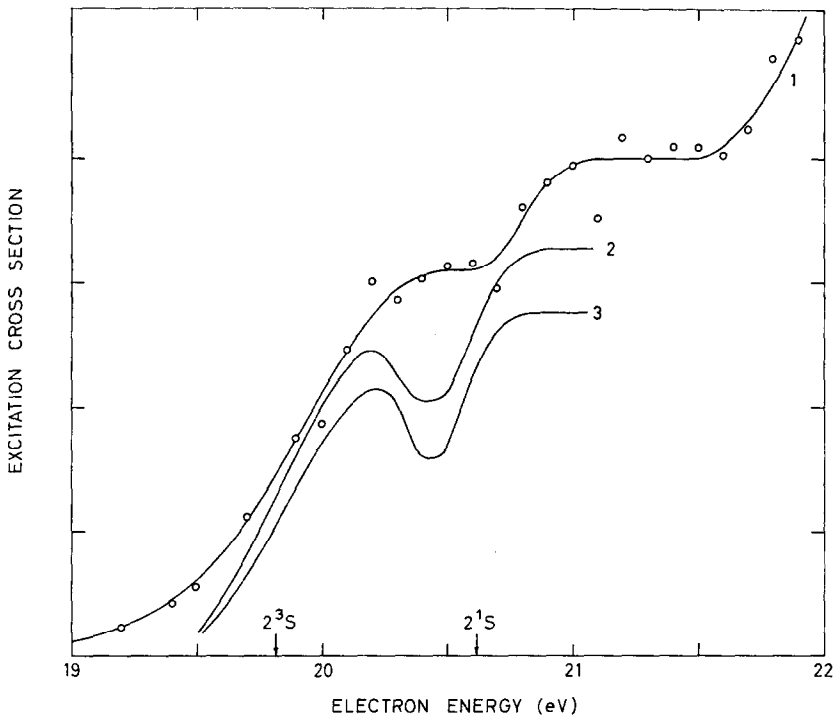

Fig. 9. One corresponding set of measured (1) and unfolded (2 and 3) functions for excitation of He to the metastable states. For this series of measurements kT was about 0.3 eV. Curves 2 and 3 are obtained with the EDD method with $\Delta V = 0.3$ and 0.1 eV, respectively (see section 8). The (arbitrary) vertical scales for curves 1, 2 and 3 are not related. The energy scale for all curves has been obtained as in fig. 8 (and therefore fig. 9 does not correspond to fig. 7). Accordingly the measurements were extended to "far" above the threshold for direct ionization, and the linear parts of the ionization functions were shifted along the energy axis until they intersected this axis at 25.14 eV. The energy scale of this figure may, however, be subject to a small systematic error because this series of measurements was interrupted between 22 and 23 eV.

intersection of the linear part of the (direct) ionization curve with the abcissa, our curves in figs. 9 and 10 shift by 0.56 eV towards lower E_e and the agreement with the other curves in fig. 10 becomes very bad.

An encouraging result is that the exponential tails for cumulative ionization (below 19 eV) and for direct ionization (between 22 and 24 eV) give the same kT. It is further encouraging that the unfolded excitation function resembles those of refs. 22 and 23.

6. *Additional remarks*

Several measurements have been made to find the best way to operate the apparatus and to check our results. We mention two interesting features.

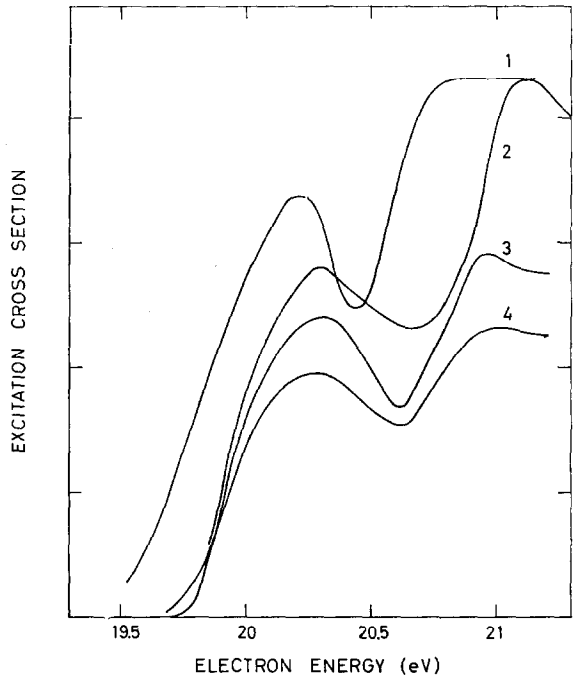

Fig. 10. Comparison of two of our unfolded functions (1 and 2) for excitation to the 2^3S and 2^1S states of He, with those of Pichanick and Simpson(3) and Schulz and Fox (4). The vertical scales are arbitrary. The energy scales of curves 1 and 2 were calibrated against the direct ionization function. Curve 1 is the same as curve 3 of fig. 9. Curve 2 is supposed to have the correct position on the energy scale; this series of measurements was not interrupted.

When measuring with two electron beams (section 3), the detected ion current was not proportional to I_{a1}. For $V_{c1}-V_{f1} \approx 20.5$ V and $I_{a1} \approx 30$ μA, the ion current even decreased with increasing I_{a1}. This "strange" behaviour must be ascribed to space charge effects; *i.e.* an increase of I_{a1} gives a larger negative space charge and consequently a shift towards lower average electron energy. Since the excitation cross sections Q_{ex} rapidly decrease (towards lower E_e) in this region, the product $I_{a1}Q_{ex}$ may be smaller at larger I_{a1}. We worked therefore in each series of measurements with constant I_{a1}.

Further, we found that varying $V_{c1}-V_{f1}$ from 25 to 50 V, with $V_{c2}-V_{f2} = 0$ V, gave an increase in background ion current at the detector. Hence, the shielding between the two collision chambers is not perfect and the signal to noise ratio decreases with increasing $V_{c1}-V_{f1}$. Therefore we did not yet measure with "high" $V_{c1}-V_{f1}$.

7. *Conclusions*

The crossed beam setup described in section 2 can succesfully be applied to measure ionization from the metastable states. For atoms our setup has some advantages as well as some disadvantages over the system in which metastables are produced in a gas discharge. For molecules both systems yield entirely different results (with respect to the preferentially excited states). With our apparatus, Bonsen[35]) already measured the ionization function of metastable $N_2(E^3 \Sigma_g^+$; excitation energy 11.87 $\pm$ 0.02 eV).

The ionization function for He 1^1S is shown to behave nonlinearly and to follow (within the experimental accuracy) Wannier's law for about the first 2.5 V above threshold. The EDD and EDD[2] methods are found to be useful in unfolding experimental excitation and ionization functions.

It is finally shown to be possible to measure cumulative ionization within one electron beam and in this way to measure (for He) the excitation function of the metastable states.

The technique of detecting metastable atoms or molecules by ionizing them with an electron beam may be useful when these metastables have low excitation energies. The usual technique, to let them impinge on a metal surface, only works well when the metastables have sufficient internal (excitation) energy to liberate secondary electrons.

APPENDIX

In sections 4 and 5 we used unfolding techniques to analyse our experimental results. In this appendix we explain these techniques. If the energy spread in the electron beam is thermal and given by eq. (6), then the relationship between the real excitation or ionization function $Q_r(E_e)$ and the measured one $Q(V)$ is given by

$$Q(V) = \beta^2 \int_V^\infty (E_e - V) \exp[-\beta(E_e - V)]\, Q_r(E_e)\, dE_e. \tag{7}$$

One can easily verify[36]) that if

$$Q_r(x) = \beta^{-2} \exp(\beta x) \frac{d^2}{dx^2} [Q(x) \exp(-\beta x)] \tag{8}$$

with $x = E_e$ is inserted in the right hand side of eq. (7), one obtains $Q(V)$. Alternatively, experimental $Q(V)$ may be used in eq. (8) to yield $Q_r(V)$. Hence if statistical errors are no problem and if one has continuous registration, one can obtain the real excitation or ionization function. In actual measurements statistical errors in general are a problem and in our measurements we had no continuous registration, but measured (counted) at intervals of 0.1 eV. We therefore did not use eq. (8) but used related methods.

The first method we used, the so called EDD method, is introduced and described by Winters *et al.*[19]).They showed that the function

$$\Delta Q(V) = [Q(V) - bQ(V + \Delta V)][1 - b]^{-1} \tag{9}$$

where $b = \exp(-\beta\Delta V)$ and ΔV has a fixed value, for example 0.1 eV, gives a much better approximation to $Q_r(E_e)$ than $Q(V)$. The electron energy distribution corresponding (see also section 4) to $\Delta Q(V)$ is

$$\Delta f(E_e - V) = [f(E_e - V) - bf(E_e - V - \Delta V)][1 - b]^{-1}. \tag{10}$$

Hence, substitution of eq. (6) gives for $V \leq E_e \leq V + \Delta V$,

$$\Delta f(E_e - V) = \beta^2(1 - b)^{-1}(E_e - V)\exp[-\beta(E_e - V)], \tag{11}$$

and for $E_e \geq V + \Delta V$,

$$\Delta f(E_e - V) = \beta^2(1 - b)^{-1}\Delta V \exp[-\beta(E_e - V)]. \tag{12}$$

For $\Delta V = 0.3$ eV, 0.2 eV and 0.1 eV we plotted this new energy distribution (multiplied with $(1 - b)$) in fig. 7. We see that the new distribution is much sharper than the original one and especially the exponential tail is greatly reduced. A great advantage of the EDD method is that it can be applied with different ΔV on one set of data. In this way a set of functions $\Delta Q(V)$ is obtained which correspond to different energy spreads. The systematic errors are smaller at smaller ΔV, but simultaneously the statistical errors are larger. By varying ΔV one can find the best compromise.

We applied the EDD method in this way to the measurements described in sections 4 and 5. The results obtained with the EDD method on the threshold behaviour for ionization from the ground state of He, essentially confirm those obtained with the EDD[2] method (see below and section 4). Some of the results obtained for cumulative ionization are shown in fig. 9.

Eqs. (8) and (9) are related via:

$$\lim_{\Delta x \to 0} \Delta Q(x) = -\beta^{-1}\exp(\beta x)\frac{d}{dx}[Q(x)\exp(-\beta x)] \tag{13}$$

where for v one may read V. Hence, the EDD method corresponds to taking the first derivative whereas in the exact expression one has to take the second derivative.

We now introduce another unfolding technique, the EDD[2] method, which is directly related to eq. (8). We define the function

$$\begin{aligned}\Delta^2 Q(V) &= [\Delta Q(V) - b\Delta Q(V + \Delta V)][1 - b]^{-1} = \\ &= [Q(V) - 2bQ(V + \Delta V) + b^2 Q(V + 2\Delta V)][1 - b]^{-2}\end{aligned} \tag{14}$$

where, as before, ΔV has a fixed value. Eqs. (8) and (14) are related via

$$\lim_{\Delta x \to 0} \Delta^2 Q(x) = Q_r(x). \tag{15}$$

The electron energy distribution corresponding to $\Delta^2 Q(V)$ is

$$\Delta^2 f(E_e - V) = [f(E_e - V) - 2bf(E_e - V - \Delta V) + \\ + b^2 f(E_e - V - 2\Delta V)] \times [1 - b]^{-2}. \quad (16)$$

Hence, for $V \leq E_e \leq V + \Delta V$,

$$\Delta^2 f(E_e - V) = \beta^2 (1 - b)^{-2} (E_e - V) \exp[-\beta(E_e - V)], \quad (17)$$

for $V + \Delta V \leq E_e \leq V + 2\Delta V$,

$$\Delta^2 f(E_e - V) = \beta^2 (1 - b)^{-2} (V + 2\Delta V - E_e) \exp[-\beta(E_e - V)] \quad (18)$$

and for $E_e \geq V + 2\Delta V$,

$$\Delta^2 f(E_e - V) = 0. \quad (19)$$

For $\Delta V = 0.1$ eV we plotted $(1 - b)^2 \Delta^2 f(E_e - V)$ in fig. 7. This new distribution does not have a tail.

In eq. (9) one takes differences between values of $Q(V)$ and $bQ(V + \Delta V)$. For our measurements (sections 4 and 5) and $\Delta V = 0.1$ eV, these values in general were only different by 20 to 40%. For a difference of 20%, the statistical errors in $\Delta Q(V)$ are about a factor 7 larger than in $Q(V)$. Further, in eq. (14) we "take differences of differences". Consequently, statistical errors manifest themselves stronger in the EDD^2 than in the EDD method. However, the statistical errors in the EDD^2 method may be reduced by taking larger steps ΔV. For example, the EDD^2 method with $\Delta V = 0.2$ eV gives only slightly larger statistical errors than the EDD method with $\Delta V = 0.1$ eV.

Acknowledgments. We are indebted to H. Wallinga and G. L. van der Heijde for valuable assistance with the measurements. This work is part of the research programme of the "Stichting voor Fundamenteel Onderzoek der Materie" and was made possible by financial support from the "Organisatie voor Zuiver Wetenschappelijk Onderzoek".

REFERENCES

1) Fite, W. L., Atomic and Molecular Processes, Ed. D. R. Bates (Academic Press, New York, 1962) p. 421.
2) Rubin, K., Perel, J. and Bederson, B., Phys. Rev. **117** (1960) 151.
3) Fite, W. L. and Brackmann, R. T., Proc. VIth Int. Conf. on Ionization Phenomena in Gases (Paris, 1963) Vol. 1, p. 21.
4) Neyaber, R., Rothe, E. W. Trujillo, S. M. and Marino, L. L., Proc. IIIrd Int. Conf. on Electronic and Atomic Collisions, London, 1963, Ed. M. R. C. McDowell (North-Holland Publ. Co.) p. 1089.

5) Dance, D. F., Harrison, M. F. A. and Rundel, R. D., Proc. Roy Soc. **A299** (1967) 525.
6) Tisone, G. and Branscomb, L. M., Phys. Rev. Letters **17** (1966) 236.
7) Dolder, K. T., Harrison, M. F. A. and Thonemann, P. C., Proc. Roy. Soc. **A264** (1961) 367.
8) Dance, D. F., Harrison, M. F. A. and Smith, A. C. H., Proc. Roy. Soc. **A290** (1966) 74.
9) Lineberger, W. C., Hooper, J. W. and McDaniel, E. W., Phys. Rev. **141** (1966) 151.
10) Foner, S. N., Adv. in Atomic and Molecular Physics, Eds. D. R. Bates and I. Estermann (Academic Press, New York, 1966) p. 385.
11) Vriens, L., Bonsen, T. F. M., Wallinga, H. and Fluit, J. M., Abstracts Vth Int. Conf. on Electronic and Atomic Collisions, Leningrad, 1967 (Publishing House Nauka) p. 58. This abstract contains our first preliminary results and a short description of the apparatus.
12) Vriens, L., Phys. Letters **8** (1964) 260.
13) Wannier, G. H., Phys. Rev. **90** (1953) 817.
14) Geltman, S., Phys. Rev. **102** (1956) 171.
15) Rudge, M. R. H. and Seaton, M. J., Proc. Roy. Soc. **A283** (1965) 262.
16) Hickam, W. M., Fox, R. E. and Kjeldaas, T., Phys. Rev. **96** (1954) 63.
17) Brion, C. E. and Thomas, G. E., Abstracts Vth Int. Conf. on Electronic and Atomic Collisions, Leningrad, 1967 (Publishing House Nauka) p. 53.
18) Fox, R. E., Hickam, W. M., Kjeldaas, T. and Grove, D. J., Phys. Rev. **84** (1951) 859; Rev. sci. Instr. **26** (1955) 1101.
19) Winters, R. E., Collins, J. H. and Courchene, W. L., J. chem. Phys. **45** (1966) 1931.
20) Maier-Leibnitz, H., Z. Phys. **95** (1936) 499.
21) Dorrestein, R., Physica **9** (1942) 447.
22) Schulz, G. J. and Fox, R. E., Phys. Rev. **106** (1957) 1179.
23) Pichanick, F. M. J. and Simpson, J. A., Phys. Rev. **168** (1968) 64.
24) Woudenberg, J. P. M. and Milatz, J. M. W., Physica 8 (1941) 871.
25) Cermak, V., J. chem. Phys. **44** (1966) 3774.
26) Holt, H. K. and Krotkov, R., Phys. Rev. **144** (1966) 82.
27) Schulz, G. J. and Philbrick, J. W., Phys. Rev. Letters **13** (1964) 477.
28) Chamberlain, G. E. and Heideman, H. G. M., Phys. Rev. Letters **15** (1965) 337; Chamberlain, G. E., Phys. Rev. **155** (1967) 46.
29) Ehrhardt, H. and Willmann, K., Z. Phys. **203** (1967) 1.
30) Daly, N. R., Rev. sci. Instr. **31** (1960) 264.
31) Von Smoluchowski, M., Ann. Physik **33** (1910) 1559.
32) Clausing, P., Physica **9** (1929) 65; Z. Phys. **66** (1930) 471.
33) Vriens, L., Proc. Phys. Soc. **89** (1966) 13; ibid. **90** (1967) 935.
34) Rapp, D. and Englander-Golden, P., J. chem. Phys. **43** (1965) 1464.
35) Bonsen, T. F. M., to be published.
36) Equation (8) is equivalent to a formula derived by S. N. Foner, A. Kossiakoff and F. T. McClure, Phys. Rev. **74** (1948) 1222; see also ref. 10.